Research Article Vol. 9, No. 2 | 1 Feb 2019 | OPTICAL MATERIALS EXPRESS 911
Optical Materials EXPRESS

High-repetition-rate laser-induced damage of indium tin oxide films and polyimide films at a 1064 nm wavelength

LIPING PENG,[1,2,3] YUAN'AN ZHAO,[1,2,4,6] XIAOFENG LIU,[1,2] YONGGANG LIU,[4] ZHAOLIANG CAO,[4,7] MEIPING ZHU,[1,2] JIANDA SHAO,[1,2,8] RUIJIN HONG,[5] CHUNXIAN TAO,[5] AND DAWEI ZHANG[5]

[1]*Laboratory of Thin Film Optics, Shanghai Institute of Optics and Fine Mechanics, Shanghai 201800, China*
[2]*Key Laboratory of Materials for High Power Laser, Chinese Academy of Sciences, Shanghai 201800, China*
[3]*University of Chinese Academy of Sciences, Beijing 100049, China*
[4]*State Key Laboratory of Applied Optics, Changchun Institute of Optics, Fine Mechanics and Physics, Chinese Academy of Sciences, Changchun 130033, China*
[5]*Engineering Research Center of Optical Instruments and Systems, Ministry of Education and Shanghai Key Laboratory of Modern Optical Systems, University of Shanghai for Science and Technology, Shanghai 200093, China*
[6]*yazhao@siom.ac.cn*
[7]*caozlok@ciomp.ac.cn*
[8]*jdshao@mail.shcnc.ac.cn*

Abstract: Experiments and thermal modeling of indium tin oxide transparent conductive thin film and polyimide alignment thin film coated on fused silica substrates damaged with a 1064 nm high-repetition-rate laser are described. High-repetition-rate laser irradiation results in damaged morphologies of the bulge at low laser power density and formation of a pit in the center of the bulge at higher laser power density. The damage process that is consistent with the observations as a function of laser power density and irradiation time is related to thermal effect. Simulation of the temperature-rise by exposure to high-repetition-rate laser describes the thermal effect with different pulse oscillation.

1. Introduction

Mechanical systems like gimbaled mirrors mostly accomplish optical beam steering and pointing in optical systems, but they suffer from the disadvantages of being large, heavy, and complex. Therefore, liquid crystal (LC) based electro optical beam steering components with a potential to replace traditional mechanical counterparts are emerging for application in various fields such as free-space optical communication [1, 2], remote sensing, optoelectronic countermeasure [3–6], and laser-based imaging system and so on [7–11]. The LC optical device mainly consists of glass substrate (SUB), indium tin oxide (ITO) transparent conductive layer, polyimide (PI) alignment layer, and LC layer. Laser induced damage processes of the different components of an LC optical device such as ITO film [12–15] and PI film [16–18] have been investigated, but mostly under the irradiation of single-pulse and multiple-pulse laser. With potential applications of LC optical devices in high power laser system, its damage process with high-repetition-rate laser should be researched. However, performance of the devices under the irradiation of high-repetition-rate laser, which is of significant use in optical beam steering systems, has been rarely focused on; hence, it is of paramount importance to study the interlayer coupling effect of LC optical devices under high-repetition-rate laser.

#352990 https://doi.org/10.1364/OME.9.000911
Journal © 2019 Received 30 Nov 2018; revised 14 Jan 2019; accepted 15 Jan 2019; published 30 Jan 2019

In this work, using the fundamental 1064 nm high-repetition-rate laser, we perform experiments of damage of the PI/ITO/SUB sample, which is composed of fused silica substrate, ITO transparent conductive thin film, and PI alignment thin film. The features of laser damage are revealed by changes in optical profiler images are presented and the possible damage process in connection with laser power density and irradiation time is surmised at the same time. Simulation of the temperature-rise produced in PI/ITO/SUB on exposure to a high-repetition-rate pulse train is performed to help understand the damage morphologies.

2. Sample preparation and experimental methods

2.1 Sample preparation

Experiments were conducted on the sample marked as PI/ITO/SUB and shown in Fig. 1, a 25-nm-thick ITO film was deposited on fused silica substrate by magnetron sputtering; effective refractive index of the film was about 1.8 [19] while the bandgap was about 4.2 eV. 80-nm-thick PI film was spin-coated on the ITO layer. Layer thicknesses were measured using stylus profiler; size of this sample was 30 mm × 30 mm × 2 mm.

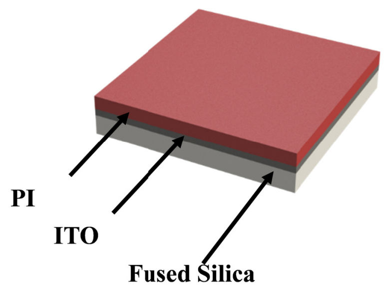

Fig. 1. Diagram showing PI/ITO/SUB sample.

2.2 Experimental setup

Figure 2 depicts the experimental setup. Laser damage experiments were conducted using a Nd:YAG high-repetition-rate laser, which produced pulses at a repetition rate of 10 kHz, the pulse width was about 300 ns. The spot diameter on target plane was 726 μm (at $1/e^2$) with Gaussian beam profile at the fundamental wavelength of 1064 nm. Laser power was adjusted using a half-wave plate and a polarizer and a power meter was employed to record it from a split-off portion of the beam. The angle of incidence was almost 0°. He-Ne laser was used as probe laser, a CCD was used to observe the radiation area, and an auxiliary estimated whether the damage occurs. The sample was held vertically with the film facing the laser and it was irradiated at five independent sites for each power density. The laser-induced damage threshold (LIDT) is the maximum incident power density when the damage occurs at a site with 0% damage possibility (W/cm^2).

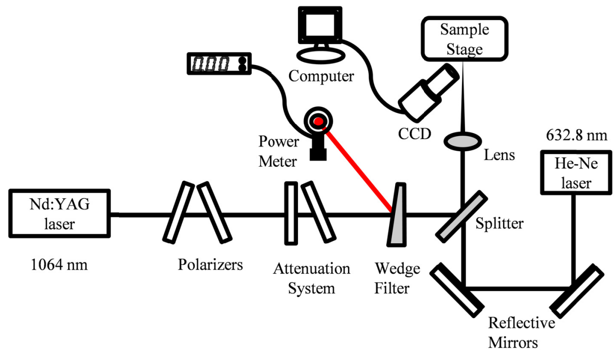

Fig. 2. Schematics of laser irradiation damage threshold measurement using high-repetition-rate laser.

2.3 Damage characterizations

For the high transmittances for fundamental wavelength and the extremely small thickness of the films, it was challenging to observe damage morphology of the sample using an optical microscope. However, the optical profiler (WYKO NT9100) proved to be significantly sensitive to detect the damage easily. The working principle of an optical profiler is based on scanning white light interferometry. It is a noncontact method for providing almost the same information as a stylus based profilometer. In our experiment, the sample tested was observed offline with the optical profiler, and the damage was defined by the deformation structures that could be distinguished from the pristine areas.

3. Temperature-rise modeling

High-repetition-rate laser is essentially a still pulse laser; however, compared to that of a pulse laser, the peak power of its single-pulse is too low to induce any damage. Therefore, the damage induced by a train of laser pulses is mainly due to the accumulation of heat. Optical damage under high-repetition-rate laser irradiation is mainly related to thermal effect [20, 21]. At this point, temperature-rise is the most important factor that induces damage in the sample [22, 23]. Therefore, we mainly simulate the temperature field with different laser parameters such as irradiation power density and irradiation time to analyze the damage mechanism.

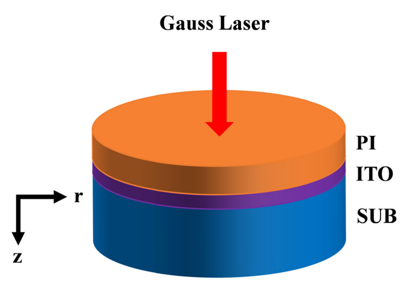

Fig. 3. Temperature-rise diagram of PI/ITO/SUB sample used for the simulation process.

Finite element simulations were performed to model the temperature-rise produced in the PI/ITO/SUB sample. A three-dimensional (3D) axisymmetric geometry was used to describe the heat source deposited into a cylindrically shaped disk 10 mm in diameter and 3 mm in thickness. Considering the structure of PI/ITO/SUB sample, a model of the multilayer material of this sample is established, as shown in Fig. 3. A high-repetition-rate laser beam has a Gaussian distribution exposure to the surface of the PI/ITO/SUB sample along the z

Optical Materials EXPRESS

direction that is perpendicular to the surface and its intensity distribution at the surface is as follows.

$$I(r,t) = [2P(t)/(\pi r_0^2)]\exp[-2(r/r_0)^2] \tag{1}$$

where r_0 is the $1/e^2$ times the radius of the Gaussian laser beam source, $P(t)$ is the deposited time-dependent laser power given by the following:

$$P(t)=\begin{cases} P_0 & \dfrac{N}{f} \le t \le \tau + \dfrac{N}{f} \\ 0 & \tau + \dfrac{N}{f} \le t \le (N+1)\dfrac{1}{f} \end{cases} \tag{2}$$

where P_0 is the peak power of each pulse, τ is the pulse width of square pulse, f is the pulse repetition rate, and N is all the number of pulses within irradiation time in one laser spot area. The temperature field of the sample as a function of time t, radial position from the center of the beam r, and vertical depth into the sample z satisfied the heat conduction equation given below [24].

$$\rho_i C_i(\partial/\partial t)T(r,z,t) = \frac{k_i}{r}(\partial^2/\partial r^2)T(r,z,t) + k_i(\partial^2/\partial z^2)T(r,z,t) + Q \tag{3}$$

where $i = 1,2,3$, stand for the parameters of PI film, ITO film, and fused silica substrate, respectively, and ρ_i, C_i, and k_i stand for the density, specific heat, and thermal conductivity of materials, respectively, $T(r,z,t)$ is the temperature field depending on r, z, and t, and Q is the surface heat source given by the equation below.

$$Q = \alpha I(r,t)(1-R) \tag{4}$$

where α is the laser absorption coefficient for 1064 nm laser and R is the reflectivity.

To simplify the temperature-rise modeling, the data used for this sample neglected any temperature dependence of these thermo-optical parameters. Heat transfer boundary conditions for laser heating problems typically include evaporative cooling, radiation, and surface convection [25], but radiative and evaporative cooling from the surface can be shown to be negligible [26, 27]. Considering the thickness of the substrate is much larger than that of ITO layer and PI layer, Dirichlet boundary condition was imposed only along the film surface and all the other mechanical boundaries were treated as air convection; these were expressed as follows.

$$-k_1\frac{\partial T(r,z=0,t)}{\partial z} = \frac{1}{\alpha}Q - \gamma(T(r,z=0,t)-T_0); \tag{5}$$

$$-k_3\frac{\partial T(r,z=h,t)}{\partial z} = -\gamma(T(r,z=h,t)-T_0); \tag{6}$$

$$-k_{1or3}\frac{\partial T(r{=}\infty,z,t)}{\partial z} = -\gamma(T(r{=}\infty,z,t)-T_0); \tag{7}$$

$$T(r,z,t=0) = T_0 \tag{8}$$

where γ is the surface heat interchange coefficient, h is the thickness of the sample, and T_0 is the initial surface temperature. Material properties were taken from the data provided by the vendor or data used in previous calculations, and are tabulated in Table 1.

Optical Materials EXPRESS

Table 1. The thermo-physical parameters of relevant materials in the sample

Material parameter	Glass[a]	ITO[a,b]	PI[c,d]
Absorption coefficient (1/cm)	0	1000	0
Density (kg/m^3)	2200	7140	1400
Heat capacity (J/kg/K)	840	340	814.5
Thermal conductivity (W/cm/K)	0.0140	0.1100	0.0015
Thickness (nm)	3×10^6	25	80

[a]From Optics Express, 25.21, 25533- (2017).
[b]From Applied Physics Letters, 34.3, 196-198, (1979).
[c]From Journal of Engineering Materials and Technology, 132.1, 011004, (2010).
[d]From Applied Physics A, 56.1, 43-50, (1993).

4. Research on the damage process that occurs due to irradiation with high repetition-rate laser

4.1 Damage process due to irradiation with a high-repetition-rate laser

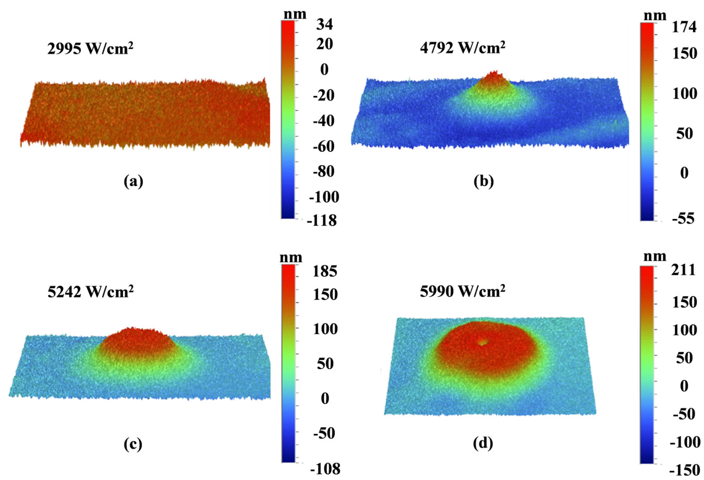

Fig. 4. The damage morphology-change with laser power density at 10 kHz repetition rate.

The typical damage morphologies of the PI/ITO/SUB sample at 10 kHz repetition rate and 120 s irradiation time were investigated across a range of laser power density values as shown in Fig. 4. The LIDT of this sample was about 2995 W/cm^2 and the apparent damage started with bulge of the sample, as shown in Fig. 4(b). The size of the bulge enlarged with increase in laser power density. When irradiated with a power density of more than 5242 W/cm^2, as shown in Fig. 4(c), a pit appeared at the center of the bulge.

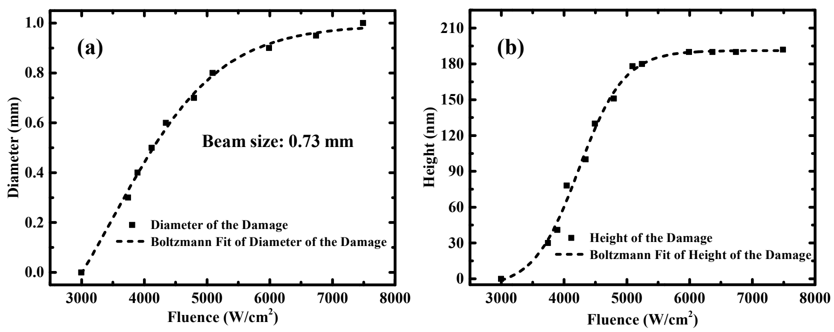

Fig. 5. The (a) damage diameter and (b) damage height of PI/ITO/SUB with respect to laser power density at a repetition rate of 10 kHz.

More statistical information of the damage morphology is depicted in Fig. 5, which clearly shows that the diameter (radial expansion) of the damage was much larger than the height (vertical expansion). As mentioned earlier, the damage is defined by the deformation structures that can be distinguished by the optical profiler from the pristine areas. The diameter is the max transverse size of one damage site and the height is the max height of one damage site. Experimental results shown in Fig. 5(a) demonstrate that the damage diameter of the sample increased with increasing laser power density, and the damage diameter did not increase obviously as the power density increased to 5242 W/cm^2. The diameter of the damage near the laser damage threshold is ~0.1 mm and the maximum diameter is about 1 mm, which was scaled out to the laser spot diameter (~0.73 mm), due to the diffusion of the thermal that absorbed by ITO film under the laser irradiation. Similarly, experimental results shown in Fig. 5(b) demonstrate that the damage height of the sample increased with increasing laser power density till the power density became 5242 W/cm^2, beyond which there was no significant change in the damage height. The height of the damage near the laser damage threshold was ~25 nm and increased to a maximum height of ~200 nm with increase in the laser power density. The morphology of the pit appeared when the laser power density was higher than 5242 W/cm^2 as illustrated in Fig. 4(c).

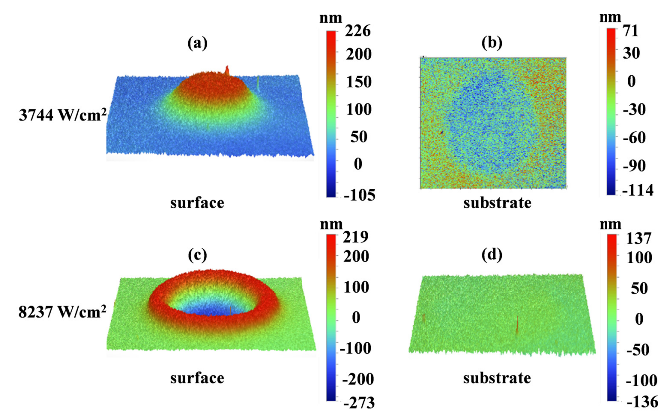

Fig. 6. Surface morphology of the film and the corresponding substrate region after removal of the film layer. (a) and (b) represent the morphology of surface of the film and backside of the substrate, respectively under irradiation with 3744 W/cm^2, (c) and (d) represent the morphology of surface of the film and backside of the substrate respectively under irradiation with 8237 W/cm^2.

Optical Materials EXPRESS

The details about bulge and pit on the surface of the sample could not be observed by scanning electron microscope (SEM) and optical microscope. In order to reveal the damage details as much as possible, we remove the damaged PI/ITO films from the surface of the sample by tweezers and then comparing compare the damage of the substrate in corresponding areas. As shown in Fig. 6, no damage was found in the substrate in the corresponding damaged regions, which demonstrated that the bulge and pit of the damage were within the PI/ITO films rather than the substrate, and the damage was related to the PI/ITO films. The circular profile on the surface of substrate as shown in Fig. 6(b) is a trace left after removal of the PI/ITO films.

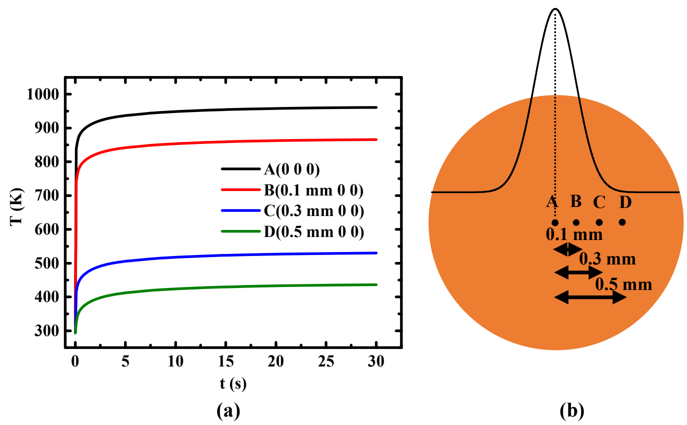

Fig. 7. Radial temperature distribution in 30 s under 3000 W/cm^2 laser irradiation in one spot area, (a) is the curve of temperature changing over time at several points in the radial direction, (b) is the distribution of several points in the radial direction and the black curve is the Gaussian distribution of the laser beam along the x direction.

The effects of temperature-rise in the sample under high-repetition-rate laser irradiation on the formation of bulge and pit were analyzed. Surface temperature of the sample rose sharply to its maximum value within about 2 s and was basically stable after about 30 s (data not shown). In this case, we only simulated temperature-rise of sample within first 30 s. The simulation results of radial temperature distribution in 30 s under 3000 W/cm^2 (near LIDT) laser irradiation are depicted in Fig. 7. The figure shows the temperature-rise at four different locations on the surface of the sample. Line A in Fig. 7(a) indicates the temperature-rise at the center of the laser spot. Lines B, C, and D indicate the temperatures at the point B, C, and D, respectively in Fig. 7. The black curve is the Gaussian distribution of the laser beam along the x direction, the center of the beam corresponds to the center of sample. As is seen from Fig. 7(a), the temperature of the surface rises rapidly in first 2 s, and eventually stabilizes within 20 s. The maximum temperature of the irradiated center of the surface was ~950 K, which was far from the melting temperature of the material (about 1900 K for ITO) [28]. For the region within ~0.1 mm radius, the temperature distinction was between 950 K and 850 K, at which the damage would just occur. For regions beyond 0.1 mm radius, the temperature decreased rapidly, and the temperature at a distance of 0.3 mm from center had reduced to about 500 K, at which the damage would not occur. Furthermore, thermosetting PI was known for thermal stability, good chemical resistance, and excellent mechanical properties, and exhibited very low creep and high tensile strength [29]. These properties were retained at temperatures as high as 673 K, but the higher irradiation laser power density resulted in thermally induced degradation when the surface temperature exceeded 923 K [27, 30], which probably resulted in material thermal deformation that manifested itself as a bulge in the surface. This should be the main reason for the damage diameter to be within ~0.1 mm under laser irradiation near damage threshold, as shown in Fig. 5(a).

Optical Materials EXPRESS

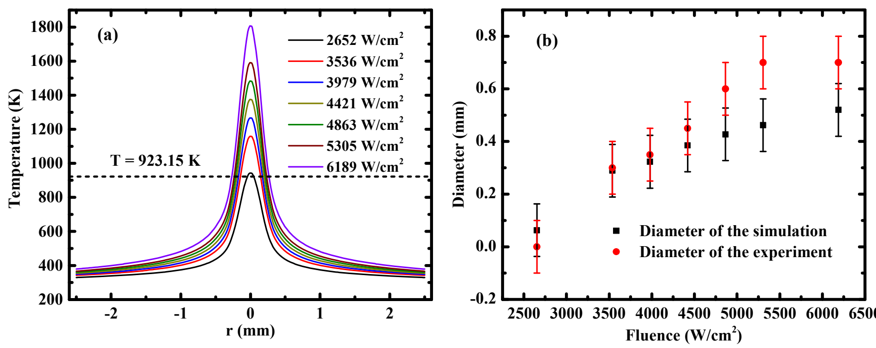

Fig. 8. (a) Temperature distribution along radial direction under a series of laser power density irradiations within 30 s. (b) Diameter of the damaged zones in PI/ITO/SUB sample as a function of irradiation power density exposure at 10 kHz.

Figure 8 shows the temperature distribution along the radial direction under a series of laser power density irradiations within 30 s and diameter of the damage zones as a function of irradiation power density. The surface temperature distribution in Fig. 8(a) is nearly a Gaussian distribution due to the Gaussian beam profile. The damage diameter in the simulation is defined as the area in which the temperature has risen above the thermal degradation temperature of PI film (923 K). Then the damage diameter in the simulation has been compared to the damage diameter in the experimental, as shown in Fig. 8(b). The black square points represent the result of simulated damage diameter, and the red round points represent the result of measured damage diameter. The comparison between simulation results and experimental results in Fig. 8(b) indicate that the area with temperature higher than 923K and the bulge area are comparable.

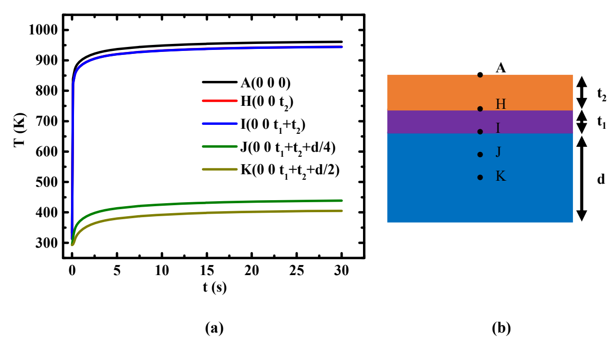

Fig. 9. Vertical temperature distribution in first 30 s under 3000 W/cm^2 laser irradiation, (a) is the curve of temperature changing over time at several points in the vertical direction, (b) is the distribution of several points in the vertical direction.

The vertical temperature distribution in first 30 s under 3000 W/cm^2 laser irradiation is depicted in Fig. 9(a), which illustrates the temperature-rise at five different locations along the z-direction. Line A in Fig. 9(a) indicates the temperature-rise at the center of the surface. Lines H, I, J, and K indicate temperatures at points 80 nm, 80 nm + 25 nm, 80 nm + 25 nm + 0.75 mm, 80 nm + 25 nm + 0.75 mm + 1.5 mm away from point A, respectively; these points are shown in Fig. 9(b). The highest temperature at all the three points A, H, and I was about 950 K; the temperature curves of H and I are nearly indistinguishable suggesting that the distinction of the temperature between the surfaces of two films was negligible. In addition, the peak temperature in the films was significantly higher than that in the substrate.

Under the irradiation of high-repetition-rate laser, ITO film is the main absorption source because of the large number of free carriers, which cause the temperature-rise. Within the irradiation time (120 s), the thermal has diffused to PI film and the substrate, which makes a small temperature-rise gradient to each layers, as shown in Fig. 9. That is to say, ITO film mainly absorbs the laser energy (servers as thermal source), PI film and the substrate diffuse thermal (server as diffusion source). However, the thermal degradation temperature of PI film is about 923 K. As the temperature rise to 923 K, the PI film is modified to carbon-like material which may cause vertical thermal deformation on the surface. As we know, PI film is thermoplastic and has good mechanical elongation [31, 32]. The temperature-rise increases with the increasing of laser power density, and then the height of the bulge damage enlarges gradually. When irradiated with a power density higher than 5242 W/cm2, as shown in Fig. 4(c), a pit appeared at the center of the bulge. We speculate that the vertical thermal deformation at higher power density cannot be maintained after the laser was stopped, and the pits formed during the cooling process after laser irradiation.

4.2 Effect of irradiation time on the damage of the sample

In order to make further investigation of the thermal incubation effect on PI/ITO/SUB sample, effect of multiple pulses was observed over a range of irradiation times (2–120 s) with a 10 kHz repetition rate, and the corresponding pulse number over a range of 2×10^4 to 1.2×10^6. Figure 10 shows typical morphologies of the damage sites produced above the LIDT within 120 s, and the process of damage generation was the same as that shown in Fig. 4. The apparent damage started with a bulge and the size of the bulge enlarged with increasing irradiation time. When irradiated for more than 20 s, a pit appeared on the center of the bulge, and its size increased with increasing irradiation time.

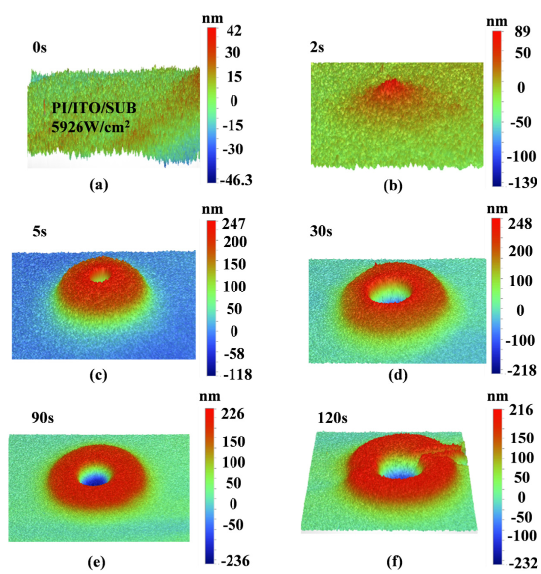

Fig. 10. The process of change in damage morphology of PI/ITO/SUB sample under 10 kHz repetition rate and 5926 W/cm^2 irradiated power density laser. (a)–(f) represent the damage morphology in the time range of 0–120 s; the morphologies were obtained using an optical profiler.

Optical Materials EXPRESS

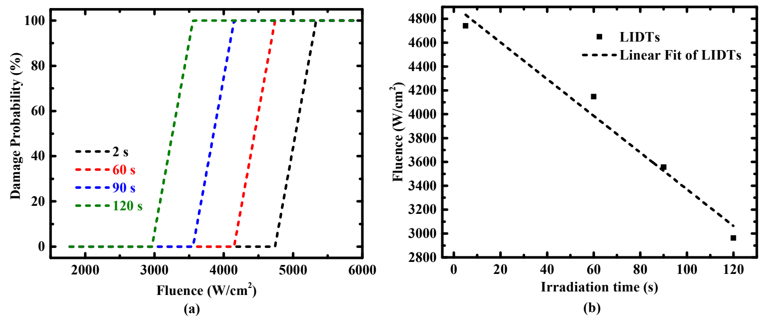

Fig. 11. (a) The relationship between the damage probability and irradiation power density in a range of irradiation times with a 10 kHz repetition rate laser. (b) The LIDT versus irradiation time.

The result of 1-on-1 test performed on the PI/ITO/SUB sample with 10 kHz repetition rate is depicted in Fig. 11. It suggests that the LIDT of this sample decreased with increasing irradiation time, which confirmed the influence of the thermal accumulation effect under high-repetition-rate laser irradiation.

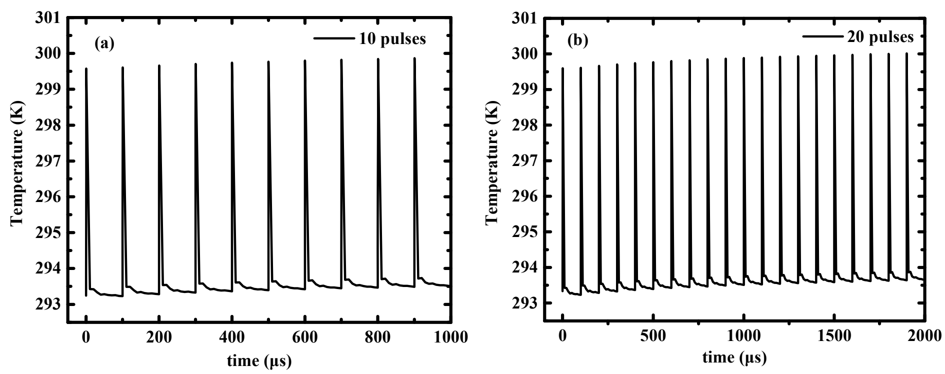

Fig. 12. The temperature-rise in case of (a) 10 pulses and (b) 20 pulses with a 10 kHz repetition rate laser irradiation.

The cumulative heating effect from a pulse train is illustrated with the simulation of temperature, and the temperature-rises when 10 and 20 pulses are applied at 10 kHz and 3000 W/cm^2 are shown in Fig. 12. There was a minute cumulative heating and the peak temperature-rise reached 299.9 K by the 10th pulse and 300.1 K by the 20th pulse. It suggested that the temperature-rise of the sample accumulates with the increase in the number of pulses, and in this case, the temperature was projected to about 690 K within 2 s (time of dramatic temperature-rise), which was insufficient to cause damage. When irradiated for longer than 2 s, the temperature-rise accumulated by laser irradiation was too small to reach the temperature than can produce damage.

5. Conclusions

We described experiments and thermal modeling of the damage of PI/ITO/SUB sample using the fundamental 1064 nm high-repetition-rate laser. Micron-scale-size bulge and pit features in this sample were observed by using optical profiler, and the morphologies were associated with laser power density and irradiation time closely. Size of the damage increased steadily to a certain value with increasing laser power density and irradiation time, but it did not degenerate into the features of thermal degradation such as melting and evaporation because of the low temperature-rise. It was found that the LIDT of this sample was related to the irradiation time, as it decreased with increasing irradiation time for the same pulse duration

Optical Materials EXPRESS

and irradiation power of single-pulse. Simulation of the temperature-rise by exposure to high-repetition-rate laser helped describe the cumulative heating effect.

Funding

National Natural Science Foundation of China (NSFC) (61308021,11774319).

References

1. W. J. Miniscalco and S. A. Lane, "Optical Space-Time Division Multiple Access," J. Lightwave Technol. **30**(11), 1771–1785 (2012).
2. L. Wu, X. Wang, C. Xiong, Z. Huang, R. Zhuo, J. Rao, and Q. Tan, "Polarization-independent two-dimensional beam steering using liquid crystal optical phased arrays," Chin. Opt. Lett. **15**(10), 101601 (2017).
3. N. N. Arev, B. F. Gorbunov, G. V. Pugachev, and Y. A. Bazlov, "Application of a laser ranging system to the metrologic certification of satellite radar measurement systems," Meas. Tech. **36**(5), 524–525 (1993).
4. M. Kleeman and U. O. Nseyo, "High-power (80-w) KTP laser vaporization of the prostate in the management of urinary retention: long-term follow up," Proceedings of SPIE - The International Society for Optical Engineering 5, 1178–1180 (2004).
5. X. Li, X. Yu, F. Chen, R. Yan, J. Gao, J. Yu, and D. Chen, "Comparison on performance of acousto-optically Q-switched Nd:GdVO4 and Nd:YVO4 lasers at high repetition rates under direct diode pumping of the emitting level," Opt. Express **17**(11), 9468–9476 (2009).
6. X. Yan, Q. Liu, X. Fu, H. Chen, M. Gong, and D. Wang, "High repetition rate dual-rod acousto-optics Q-switched composite Nd:YVO4 laser," Opt. Express **17**(24), 21956–21968 (2009).
7. B. Winker, M. Mahajan, and M. Hunwardsen, "Liquid crystal beam directors for airborne free-space optical communications," in Aerospace Conference 2004, 631–634.
8. M. A. Maun and P. B. Cavers, "Voltage calibration of dual-frequency liquid crystal devices for infrared beam steering applications," Proc. SPIE **5892**, 202–204 (2005).
9. Z. Jian, F. Yun, W. Liying, and X. Lin, "Liquid Crystal Beam Steering Technologies," Chin. J. Lasers **37**(2), 325–334 (2010).
10. F. Xiao and L. Kong, "Angular magnification method of liquid crystal optical phased array based on telescope system," in *International Symposium on Photoelectronic Detection and Imaging 2013: Laser Communication Technologies and Systems* (2013), pp. 165–189.
11. X. He, X. Wang, L. Wu, Q. Tan, M. Li, J. Shang, S. Wu, and Z. Huang, "Theoretical modeling on the laser induced effect of liquid crystal optical phased beam steering," Opt. Commun. **382**, 437–443 (2017).
12. J. H. Yoo, J. J. Adams, M. G. Menor, T. Y. Olson, J. R. I. Lee, A. Samanta, J. Bude, and S. Elhadj, "Nanosecond laser-induced damage of transparent conducting ITO film at 1064 nm," Laser-Induced Damage in Optical Materials **2016**, 10014 (2016).
13. J. H. Yoo, M. G. Menor, J. J. Adams, R. N. Raman, J. R. Lee, T. Y. Olson, N. Shen, J. Suh, S. G. Demos, J. Bude, and S. Elhadj, "Laser damage mechanisms in conductive widegap semiconductor films," Opt. Express **24**(16), 17616–17634 (2016).
14. C. W. Cheng, I. M. Lee, and J. S. Chen, "Femtosecond laser processing of indium-tin-oxide thin films," Opt. Lasers Eng. **69**, 1–6 (2015).
15. J.-H. Yoo, A. Lange, J. Bude, and S. Elhadj, "Optical and electrical properties of indium tin oxide films near their laser damage threshold," Opt. Mater. Express **7**(3), 817–826 (2017).
16. K. L. Marshall, J. Gan, G. Mitchell, S. Papernov, A. L. Rigatti, A. W. Schmid, and S. D. Jacobs, "Laser-damage-resistant photoalignment layers for high-peak-power liquid crystal device applications," Proceedings of SPIE - The International Society for Optical Engineering 7050(2008).
17. K. L. Marshall, C. Dorrer, and S. H. Chen, "Photo-aligned liquid crystal devices for high-peak-power laser applications," Liq. Cryst. **XVI**, 84750U (2012).
18. X. Liu, Y. Xiong, R. Wang, J. Yang, G. Wu, and N. Ren, "Laser etching of aluminum thin film on polyimide: Simulation and experimental studies," Surf. Coat. Tech. **277**, 107–116 (2015).
19. W. T. Pawlewicz, I. B. Mann, W. H. Lowdermilk, and D. Milam, "Laser-damage-resistant transparent conductive indium tin oxide coatings," Appl. Phys. Lett. **34**(3), 196–198 (1979).
20. M. Mansuripur, G. A. Connell, and J. W. Goodman, "Laser-induced local heating of multilayers," Appl. Opt. **21**(6), 1106–1114 (1982).
21. M. F. Koldunov, A. A. Manenkov, and I. L. Pokotilo, "Multishot laser-induced damage in optical materials: an analysis of main regularities," Proc. SPIE **3244**, 641–649 (1998).
22. F. Dai, S. Xiong, and Z. Gong, "The temperature rise in films at the repeat rate pulse laser irradiation determined based on finite element method," Spacecraft Environment Engineering **7019**, 701924 (2009).
23. A. Manenkov, G. Matyushin, V. Nechitailo, A. Prokhorov, and A. Tsaprilov, "On the nature of the accumulation effect in laser-induced damage to optical materials," Opt. Eng. **22**(4), 224400 (1983).
24. Z. Jia, T. Zhang, H. Zhu, Z. Li, Z. Shen, J. Lu, and X. Ni, "Stress damage process of silicon wafer under millisecond laser irradiation," Chin. Opt. Lett. **16**(1), 011404 (2018).

Optical Materials EXPRESS

25. M. J. Matthews, S. T. Yang, N. Shen, S. Elhadj, R. N. Raman, G. Guss, I. L. Bass, M. C. Nostrand, and P. J. Wegner, "Micro-shaping, polishing, and damage repair of fused silica surfaces using focused infrared laser beams," Adv. Eng. Mater. **17**(3), 247–252 (2015).
26. R. M. Vignes, T. F. Soules, J. S. Stolken, R. R. Settgast, S. Elhadj, and M. J. Matthews, "Thermomechanical modeling of laser-induced structural relaxation and deformation of glass: volume changes in fused silica at high temperatures," J. Am. Ceram. Soc. **96**(1), 137–145 (2013).
27. P. E. Dyer, M. Pervolaraki, and T. Lippert, "Experimental studies and thermal modelling of 1064- and 532-nm Nd:YVO 4 micro-laser ablation of polyimide," Appl. Phys., A Mater. Sci. Process. **80**(3), 529–536 (2005).
28. O. Yavas and M. Takai, "Effect of substrate absorption on the efficiency of laser patterning of indium tin oxide thin films," J. Appl. Phys. **85**(8), 4207–4212 (1999).
29. M. K. Khosa, M. A. Jamal, R. Iqbal, M. Muneer, M. J. Saif, K. M. Zia, and M. Hamid, "Thermal stability and mechanical properties of organo-soluble and processable polyimides for high-temperature materials," Journal of Macromolecular Science: Part D - Reviews in Polymer Processing **56**, 22–28 (2016).
30. Z. Ball, T. Feurer, D. L. Callahan, and R. Sauerbrey, "Thermal and mechanical coupling between successive pulses in KrF-excimer-laser ablation of polyimide," Appl. Phys., A Mater. Sci. Process. **62**(3), 203–211 (1996).
31. X. Kong, F. Teng, H. Tang, L. Dong, and Z. Feng, "Miscibility and crystallization behaviour of poly (ether ether ketone)/polyimide blends," Polymer (Guildf.) **37**(9), 1751–1755 (1996).
32. P. C. Irwin, Y. Cao, A. Bansal, *et al*., "Thermal and mechanical properties of polyimide nanocomposites," Electrical Insulation and Dielectric Phenomena, Annual Report. Conference on. IEEE, 120–123 (2003).